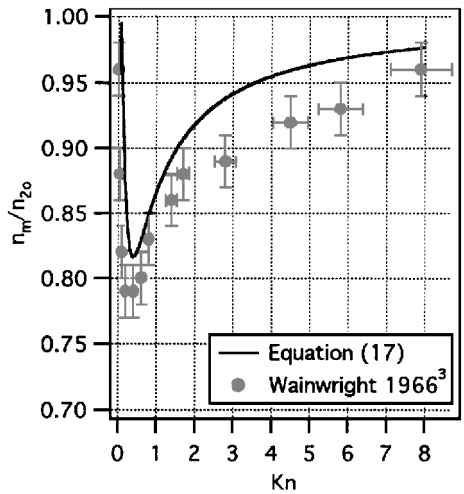

Fig. 1 Comparison of front face scattering data from Wainwright and Rogers[3] with Eq. (17) for a constant C_1 = 0.4 (error bars added to reflect uncertainty in reading data from original paper).

where the constant κ is defined as

$$\kappa \equiv \frac{mu_o^2}{mu_o^2 + \frac{1}{2}u_o\sqrt{2\pi mkT_p}} \tag{16}$$

Discussion

The model as presented has some intriguing qualities. If we assume that the depth of the collision sheath scales with a physical length scale in the flow so that $L/\lambda = Kn^{-1}$, Eq. (17) can be compared directly with data obtained by Wainwright and Roger.[3] Because the parameter L was only loosely defined, we are free to insert a constant C_1 in front of it as a free parameter and should expect the value of the constant to be on the order of unity:

$$n_m/n_{2o} = 1 - \tfrac{1}{2}(C_1 L/\lambda)e^{-(C_1 L/\lambda)} \tag{17}$$

Wainwright and Roger used impact probes of varying size and with different probe face geometries to quantify the effect of molecular scattering at transitional Knudsen numbers. Figure 1 compares Wainwright's data with Eq. (17) for a value of $C_1 = 0.4$, with L equal to the diameter of the impact probe face. The agreement between Eq. (17) and the data is excellent. The relative difference between the two is less than 4%. The largest effect of intermolecular collisions occurs expectedly in the regime of $0.5 < Kn < 1$. As the Knudsen number further increases, and the flow approaches free molecular, the ratio of measured density to freestream density tends toward unity. This is expected because the molecules will no longer scatter at such large relative mean free paths and the incident and reflected streams will move through each other unperturbed.

Acknowledgments

This work was sponsored by the NASA Johnson Space Center (JSC) under Contract NAG9-709. This support is gratefully acknowledged. The authors would like to thank Ricardo Machin of JSC (Contract Monitor) for his assistance and advice, as well as Steve Fitzgerald.

References

[1]Fitzgerald, S. M., Rocha, R. A., Bouslog, S. A., Hughes, J. R., and Leahy, K. S., "Far Field Plume Characterization Testing in Support of Space Station Plume Impingement Methodology Validation," AIAA Paper 94-2636, June 1993.

[2]Gombosi, T. I., *Gaskinetic Theory*, Cambridge Univ. Press, Cambridge, England, UK, 1994.

[3]Wainwright, J. B., and Roger, K. W., "Impact Pressure Probe Response Characteristics in High Speed Flows with Transition Knudsen Numbers," *Proceedings of 4th International Symposium on Rarefied Gas Dynamics*, edited by J. H. deLeeuw, Vol. 2, 1966, pp. 151–174.

G. Laufer
Associate Editor

Attenuation of Shock Waves in Gas-Particle Mixtures

H. K. Das* and J. Kurian†
Indian Institute of Technology, Madras 600036, India

Introduction

SHOCK waves formed within a gas-particle mixture have characteristics different from the pure gas case. Decay of the shock wave has been studied by a number of researchers applying different numerical methods. Compared with theoretical investigations, only a few experimental works are reported on the study of shock wave attenuation. Sommerfeld and Gronig,[1] Sommerfeld,[2] and Igra et al.[3] conducted experiments on a vertical shock tube along with numerical calculation. Olim et al.[4] and Aizik et al.[5] compared their numerical results with the experimental results of Sommerfeld.[2] The purpose of the present Note is to add more experimental results on decay process of shock waves in gas-particle mixtures inside a shock tube.

Details of Experiments

The experiments were conducted with a stainless steel horizontal shock tube 50 mm in diameter and 6 m long. The driven section is 4.5 m long and the diaphragms used were of aluminum foil. Diaphragms of different thicknesses from 0.05 to 0.25 mm were used. Rupture of a diaphragm was accomplished with high pressure on the driver side. A particle injection system was designed to produce a uniform flow rate of particles fed into the driven section immediately downstream of the diaphragm before each shock tube run. The injection system consisted of an inlet system, a particle reservoir, a convergent-divergent(CD) nozzle, a mixing chamber, and an exhaust system. The exit of the particle reservoir was placed in the diverging portion of the CD nozzle, causing particles to get sucked in by the low pressure created in the airstream when a sufficiently high-pressure air was fed into the inlet system. Particles were mixed with air in the mixing chamber and the gas-particle mixture was fed to the shock tube immediately after the diaphragm. The particles used in the experiments were Ballotini spheriglass and precipitated calcium carbonate powder. Particle material densities were 2500 and 2790 kg/m^3, respectively. Both types of particles had size distributions and average particle sizes were determined using a Malvern laser diffraction particle sizer. Mean diameter for calcium carbonate powder was 6.9 μm and that of glass particles was 34.4 μm. Photomicrographs of the particles showed the shape of the particles to be very nearly spherical.

Laser Light Extinction Technique

A beam of light from a continuous wave, He-Ne laser is made to transverse the shock-tube test section and to fall on a photodetector. The intensity of the laser beam was measured before the start of the gas-particle injection as I_0. With the gas-particle flow in the test section, the intensity is reduced to I, which is related to the initial intensity by the Lambert–Beer equation as

$$I/I_0 = \exp(-k\rho_p) \tag{1}$$

where k is a constant that includes the extinction coefficient and ρ_p is the cloud density. In the present experiments, a pin photodiode (PIN SPOT 8D, United Detector Technology) is employed as a photodetector. The output voltage E of the photodiode is directly proportional to the intensity of light incident on it. Hence, the expression of Beer's law can be written as the ratio of the voltage

Received April 30, 1996; revision received Oct. 1, 1996; accepted for publication Oct. 8, 1996; also published in *AIAA Journal on Disc*, Volume 2, Number 2.

*Research Scholar, Department of Aerospace Engineering.
†Associate Professor, Department of Aerospace Engineering.

outputs from the photodiode with and without particles in the flow as

$$E/E_0 = \exp(-k\rho_p) \tag{2}$$

The loading ratio of the gas-particle mixture was determined measuring the particle concentration obtained from laser extinction measurements at two stations along the length of the driven section. Calibration of loading ratio η was done in a calibration device that has the same cross-sectional diameter as that of the shock tube. A measured mass of particles was dispersed in the known volume of the calibration device. A digital storage oscilloscope was employed for recording the signals and values of $-\ln(E/E_0)$, which were plotted against known mass of particles, hence known loading ratio. The estimated uncertainty was $\pm 9.97\%$ for η. To obtain shock velocities from a time–distance method, four microsecond counters were used. A Lecroy data acquisition system was used to capture pressure signals from four transducers. Shock Mach numbers were calculated from shock velocities and pressure jumps after the shock. The error in the measurement of Mach numbers was $\pm 0.5\%$.

Results and Discussion

Prior to each run, the interior surface of the driven section of the shock tube was cleaned. For each type of particle, runs were made with four Mach numbers and three loading ratios. The values of photodiode output voltage before and after particle injection were used to calculate the loading ratio. Mach numbers from shock velocities were based on sound speed in pure gas.

Initial Mach number was calculated from the ratio of driver pressure and the driven pressure. A Pennwalt (model 62B-5B-0120D) and a Bourdon pressure gauge were used to measure the driven and driver pressure, respectively. The uncertainty in the magnitude of M_0 was $\pm 0.9\%$.

The shock wave attenuation results were compared with numerically predicted values of a general attenuation law proposed by Aizik et al.[5] Comparisons for three initial Mach numbers for three different loading ratios are shown in Fig. 1. Numerical predictions are closer to experimental values for glass particles. Deviation from experimental results is noticeable for the case of calcium carbonate particles whose average diameters are very small. This is because the general attenuation law is not valid for particle diameters less than 25 μm. However, considering the assumptions in the numerical calculations, the comparison is quite satisfactory.

Experimental results of shock wave attenuations at different loading ratios are shown in Fig. 2. It is clear from Fig. 2 that, for both types of particles, shock wave attenuation is greater with increasing loading ratio. In Fig. 1 for the case of initial Mach number = 1.7, the experimental attenuation result for calcium carbonate particles having smaller diameter is more steep than that for glass particles. The rate of decay for all incident Mach numbers is quite similar. Shock wave attenuation is greater for higher loading ratios. This observation was also made by Olim et al.[4] in their numerical investigation.

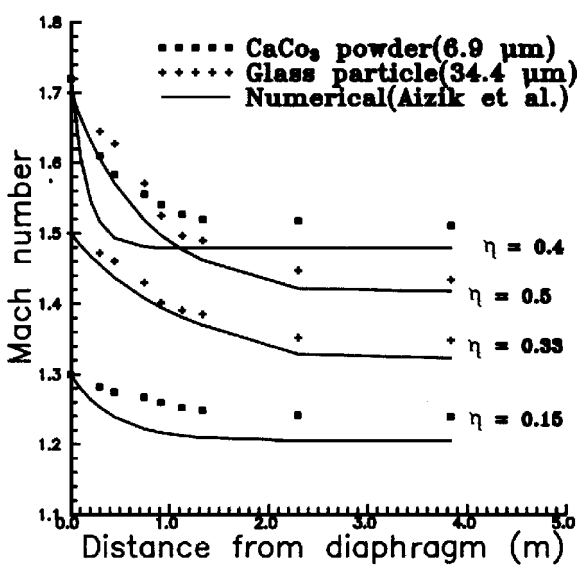

Fig. 1 Comparison of the measurements with attenuation law.

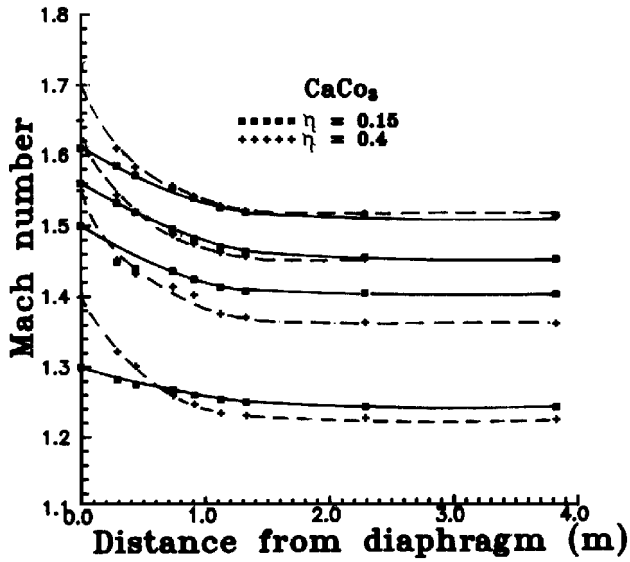

a) Calcium carbonate powder

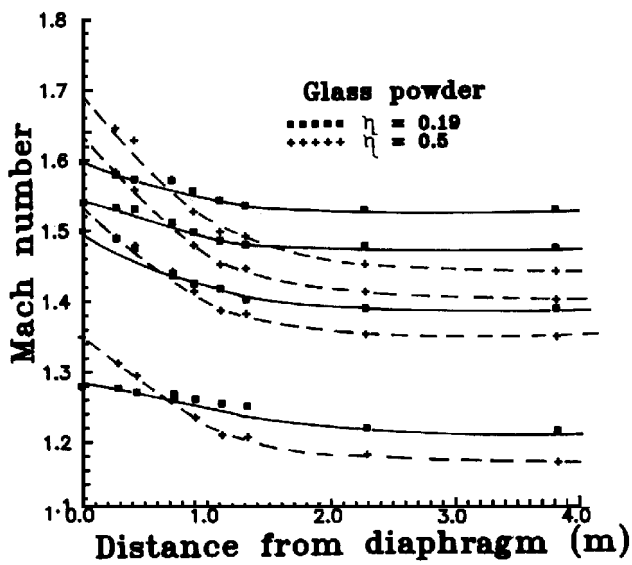

b) Glass powder

Fig. 2 Measured variation of Mach number along the length of shock tube.

Conclusion

Experimental results of shock wave attenuation in a gas-particle mixture are obtained for two types of particles with different loading ratios and incident Mach numbers. For calcium carbonate powder having very small average diameter, it is noticed that attenuation is greater than that of particles having larger average diameter. An attenuation law based on numerical prediction has been used to compare the experimental results. Good agreement is found in the case of higher size particles. However, deviation is more for very small size particles.

References

[1] Sommerfeld, M., and Gronig, H., "Decay of Shock Waves in a Dusty-Gas Shock Tubes with Different Configurations," *Proceedings of the 14th International Symposium on Shock Tubes and Waves*, Sydney Shock Tube Sym. Publishers, 1983, pp. 470–477.

[2] Sommerfeld, M., "The Unsteadiness of Shock Waves Propagating Through Gas-Particle Mixtures," *Experiments in Fluids*, Vol. 3, No. 3, 1985, pp. 197–206.

[3]Igra, O., Ben-Dor, G., Aizik, F., and Gelfand, B., "Experimental and Numerical Investigation of Shock Wave Attenuation in Dust-Gas Suspensions," *Proceedings of the 19th International Symposium on Shock Tubes and Waves* (Marseille, France), Springer, Germany, 1993, pp. 49–54.

[4]Olim, M., Igra, O., Mond, M., and Ben-Dor, G., "A General Attenuation Law of Moderate Planar Shock Waves Propagating into Dusty Gases," *Proceedings of the 18th International Symposium on Shock Tubes and Waves*, Springer–Verlag, New York, 1991, pp. 217–225.

[5]Aizik, F., Ben-Dor, G., Elperin, T., Igra, O., Mond, M., and Gronig, H., "Attenuation Law of Planar Shock Waves Propagating Through Dust-Gas Suspensions," *AIAA Journal*, Vol. 33, No. 5, 1995, pp. 953–955.

G. Laufer
Associate Editor

Effect of Loading Parameters on Damage-Induced Shear-Extension Coupling in Laminate

Y. A. Dzenis*
University of Nebraska, Lincoln, Nebraska 68588-0347
and
S. P. Joshi†
University of Texas at Arlington, Arlington, Texas 76019

Introduction

MATERIAL anisotropy is an important issue in composite structural design. It was shown in Refs. 1 and 2 that shear-extension coupling can appear in an initially balanced laminate due to unequal damage accumulation in plies with opposite orientation under the shear loading and that this may result in significant reduction of laminate shear strength. The effects of intrinsic factors such as angle-ply orientation and the presence of 0-deg plies on damage-induced anisotropy in laminates are studied in Ref. 3. The objective of this Note is to investigate the effects of extrinsic factors, i.e., the combination of shear and tensile/compressive loading as well as loading rate and deviation.

A stochastic damage accumulation model developed in Refs. 1 and 2 is used in the analysis. Random quasistationary in-plane loading is defined as a Gaussian process with autocorrelation time τ_0 and standard deviation σ_i. Stochastic function theory, the theory of excursions of random process beyond the limits as a strain failure criterion, is applied to estimate the probabilities of failure in plies. Three modes of failure, i.e., fiber breakage, matrix transverse failure, and matrix or interface shear cracking, are taken into account. Calculated probabilities are utilized in reducing ply stiffness. A brief description of the mathematical formulation of the model is given in the following paragraphs. The detailed model description is presented in Refs. 1 and 2.

Consider an orthotropic laminated composite consisting of unidirectionally reinforced plies with initial stochastic elastic material properties $\tilde{E}^k_{1_0}$, $\tilde{E}^k_{2_0}$, $\tilde{G}^k_{12_0}$, $\tilde{\nu}^k_{12_0}$. Index k denotes the ply number. Laminate lay up is described by ply orientation angles α^k and ply thicknesses h^k. Load increment applied to a laminate results in a random stress–strain field in each ply. Even at very low levels of applied load, a nonzero probability of ply failure exists and damages start to accumulate in the composite. Accumulation of damages causes a reduction in laminate stiffness and a redistribution of stresses among plies.

Received Dec. 15, 1995; revision received Oct. 9, 1996; accepted for publication Dec. 26, 1996; also published in *AIAA Journal on Disc*, Volume 2, Number 2.

*Assistant Professor, Department of Engineering Mechanics. Member AIAA.

†Professor, Center for Composite Materials, Department of Mechanical and Aerospace Engineering. Member AIAA.

Assume that in-plane stresses applied to a composite are monotonically increasing functions of a parameter t, $\bar{\sigma}_i(t) = [\sigma_{11}(t), \sigma_{22}(t), \sigma_{12}(t)]$, with parametric derivatives $\dot{\bar{\sigma}}_i(t)$. Random deformations of the composite then can be calculated by using integral equations:

$$\tilde{\varepsilon}_i(t) = \int_0^t \tilde{S}_{ij}(\tau)\dot{\sigma}_j(\tau)\mathrm{d}\tau \tag{1}$$

where $\tilde{S}_{ij}$ are current effective laminate compliances. They depend on lamina current elastic properties and composite lay up:

$$\tilde{S}_{ij}(\tau) = L\left[\tilde{E}^k_1(\tau), \tilde{E}^k_2(\tau), \tilde{G}^k_{12}(\tau), \tilde{\nu}^k_{12}(\tau), \alpha^k\right] \tag{2}$$

The current elastic constants of plies are functions of the initial elastic constants and the current damage functions:

$$\tilde{E}^k_1(\tau), \tilde{E}^k_2(\tau), \tilde{G}^k_{12}(\tau), \tilde{\nu}^k_{12}(\tau) = M\left[\tilde{E}^k_{1_0}, \tilde{E}^k_{2_0}, \tilde{G}^k_{12_0}, \tilde{\nu}^k_{12_0}, r^k_i(\tau)\right] \tag{3}$$

Damage functions may be calculated by using ply random stress–strain field parameters and some appropriate failure criteria:

$$r^k_i(\tau) = R\left[\tilde{\varepsilon}^k_i(\tau), \tilde{\sigma}^k_i(\tau)\right] \tag{4}$$

Ply stress–strain field parameters are calculated, in turn, from known composite strains $\tilde{\varepsilon}_i$ [Eq. (1)]:

$$\begin{aligned} \tilde{\varepsilon}^k_i(\tau) &= K\left[\tilde{\varepsilon}_i(\tau), \alpha^k\right] \\ \tilde{\sigma}^k_i(\tau) &= P\left[\tilde{\varepsilon}^k_i(\tau), \tilde{E}^k_1(\tau), \tilde{E}^k_2(\tau), \tilde{G}^k_{12}(\tau), \tilde{\nu}^k_{12}(\tau)\right] \end{aligned} \tag{5}$$

L, M, R, K, and P are stochastic functional operators to be specified. According to this approach, current composite elastic properties and, therefore, composite deformations and damage functions are dependent on loading history. To integrate Eq. (1), we need to calculate the stochastic stress–strain field that depends on the stochastic material properties and the deformation history. The failure criterion [Eq. (4)] should be chosen to obtain damage functions. The stiffness reduction algorithm due to damage accumulation in plies [Eq. (3)] has to be specified. The failure criterion and the stiffness reduction algorithm are described in Ref. 1.

A numerical algorithm and computer code for damage evolution and deformation history prediction in laminates subjected to general in-plane loading are developed in *Mathematica*®. In this Note, the model mentioned earlier is applied to analyze the behavior of $[\pm 30]_s$ Kevlar®/epoxy laminate under combined shear and tension/compression at various loading rates and deviations. The properties of the unidirectional Kevlar/epoxy lamina used in the calculations are given in Ref. 1.

Results and Discussion

Results of analysis of the effect of shear load in conjunction with longitudinal in-plane loading on damage-induced shear-extension coupling are shown in Tables 1–3. Table 1 corresponds to combined shear/tension $\{\sigma_{xx}, 0, \tau_{xy}\}$, Table 2 corresponds to combined shear/compression $\{-\sigma_{xx}, 0, \tau_{xy}\}$, and Table 3 corresponds to combined shear/biaxial tension $\{\sigma_{xx}, \sigma_{yy} = \sigma_{xx}, \tau_{xy}\}$. The A_{16}/A_{66} and A_{26}/A_{66} variables represent maximal relative shear-extension coupling coefficients of the in-plane stiffness matrix of laminate at failure, and S_{xy} and S^l_{xy} correspond to laminate average shear stress at failure calculated with and without taking into account damage-induced anisotropy, respectively. The final laminate failure corresponds to the shear stress when any one of the apparent moduli of the laminate becomes vanishingly small. The shear strength of the angle-ply laminate, S_{xy}, obtained by using the maximum strain criterion, is also included for reference. The ply-by-ply failure procedure described in Ref. 4 is utilized for calculating S_{xy}. The laminate is assumed to be failed when fiber and matrix in each ply is failed according to the maximum strain criterion. Note that the direct comparison between the strength prediction by the model (S_{xy} and S^l_{xy}) and the maximum strain criterion ($\hat{S}_{xy}$) is not possible because the effect of the loading rate cannot be accounted for in the maximum strain criterion. Obviously, the strengths are higher at the higher loading rates.[1]